Received September 25, 2021, accepted October 8, 2021, date of publication October 25, 2021,
date of current version November 22, 2021.

Digital Object Identifier 10.1109/ACCESS.2021.3122399

Capacity Analysis of NOMA-Enabled Underwater VLC Networks

MOHAMMED ELAMASSIE[1], (Senior Member, IEEE), LINA BARIAH[2], (Senior Member, IEEE), MURAT UYSAL[1], (Fellow, IEEE), SAMI MUHAIDAT[2,3], (Senior Member, IEEE), AND PASCHALIS C. SOFOTASIOS[2,4], (Senior Member, IEEE)

[1]Department of Electrical and Electronics Engineering, Özyeğin University, 34794 Istanbul, Turkey
[2]KU Center for Cyber-Physical Systems, Khalifa University, Abu Dhabi 127 788, United Arab Emirates
[3]Department of Systems and Computer Engineering, Carleton University, Ottawa, ON K1S 5B6, Canada
[4]Department of Electrical Engineering, Tampere University, 33101 Tampere, Finland

Corresponding author: Lina Bariah (lina.bariah@ieee.org)

ABSTRACT Visible light communication (VLC) has recently emerged as an enabling technology for high capacity underwater wireless sensor networks. Non-orthogonal multiple access (NOMA) has been also proven capable of handling a massive number of sensor nodes while increasing the sum capacity. In this paper, we consider a VLC-based underwater sensor network where a clusterhead communicates with several underwater sensor nodes based on NOMA. We derive a closed-form expression for the NOMA system capacity over underwater turbulence channels modeled by lognormal distribution. NOMA sum capacity in the absence of underwater optical turbulence is also considered as a benchmark. Our results reveal that the overall capacity of NOMA-enabled Underwater VLC networks is significantly affected by the propagation distance in underwater environments. As a result, effective wireless transmission at high and moderate spectral efficiency levels can be practically achieved in underwater environments only in the context of local area networks. Moreover, we compare the achievable capacity of NOMA system with its counterpart, i.e., orthogonal frequency division multiple access (OFDMA). Our results reveal that NOMA system is not only characterized by achieving higher sum capacity than the sum capacity of its counterpart, OFDMA system. It is also shown that the distances between sensor nodes and the clusterhead for achieving the highest sum capacity in these two multiple access systems are different.

INDEX TERMS Sum capacity, asymptotic sum capacity, non-orthogonal multiple access, orthogonal frequency division multiple access, lognormal fading, underwater optical turbulence, underwater visible light communication.

I. INTRODUCTION

The increased use of underwater sensor networks (USNs) for various applications such as environmental monitoring, oil exploration, port security, data collection, and tactical surveillance has prompted researchers to investigate underwater wireless connectivity solutions [1]. Acoustic communications have been a common choice for USNs and they can support transmission distances of up to tens of kilometers, albeit at low data rates on the order of kbps. Underwater visible light communication (UVLC) has been proposed as a complementary connectivity solution with data rates in the order of tens of Mbps [2]. As light propagates through water, it suffers from significant attenuation, especially for ultraviolet and infrared wavelengths [3]. Blue-green part of the visible light spectrum is the best wavelength for underwater transmission. While the green part of the spectrum has less attenuation in coastal water, the blue part of the spectrum is more favorable in the open ocean [4].

There has been a growing literature on UVLC where blue or green colored lasers or LEDs are used as wireless transmitters [5]–[29]. Most of these analyses are, however, limited to single user and point-to-point links. Yet, practical implementation of USNs requires the design of multiple access systems for supporting several sensor nodes. Motivated by this, some multiple access schemes for UVLC systems have been further proposed [30]–[39]. For example, in [30], an orthogonal frequency division multiplexing (OFDM)-based multiuser multiple-input multiple-output (MU-MIMO) system was investigated in the context of UVLC. They considered

The associate editor coordinating the review of this manuscript and approving it for publication was Joewono Widjaja.

linear pre-coding to serve multiple users at a time. In [32], a shot noise limited interleaver iterative non-orthogonal multiple access (NOMA) UVLC system based on a photon counting receiver is proposed. They have applied repetition coding in order to improve the performance. An orthogonal frequency division multiple access (OFDMA) UVLC system was proposed in [33] where the overall data rate is maximized subject to two constraints, namely the bit error rate (BER) for each user does not exceed the predetermined maximum BER as well as per user data rate is identical for all users. In [36], experimental validation of NOMA UVLC with blue Laser source has been demonstrated, where the sum rate of 4.686 Gbps has been achieved for two users. Another experimental validation of NOMA Underwater VLC has been demonstrated in [37]. They have compared experimentally the error rate performance of the NOMA system in air and underwater environments and demonstrated that the NOMA system works better in underwater environment.[1]

Unlike OFDMA where nodes are allocated orthogonal resources in frequency domain, in NOMA schemes, multiple users simultaneously share the entire available frequency and time resources, with a controlled interference threshold, leading to low latency and significant gains in spectral efficiency [42]. NOMA controlled interference can be realized either in power or code domains. In power-domain NOMA, users are assigned different power levels while, in the code-domain NOMA, multiplexing can be carried out using spreading sequences, which is similar to code division multiple access (CDMA) technology. Generally, power allocation in the commonly adopted NOMA systems is determined based on the channels condition between the transmitter and the receiving nodes. In specific, nodes with strong channel gains are allocated lower power coefficients, while high power coefficients are assigned to nodes with weak channel gain. For reliable data detection, each node in the USN performs successive interference cancellation (SIC) to reduce the multi-user interference. In particular, nodes successively cancel out the interference from those signals with higher power, and then decode their own signals.

In [31], the capacity of multiuser power domain NOMA was investigated numerically over lognormal fading channel, which is typically valid for weak turbulence conditions as experimentally demonstrated in [10], [43]. In [34], the authors provided a numerical evaluation for the capacity and outage probability of power domain NOMA-enabled UVLC system over lognormal fading channels and showed that NOMA outperforms OFDMA in terms of achievable capacity. The authors in [35] investigated the error rate performance and the achievable capacity of power domain NOMA-based UVLC system over Exponential-Generalized Gamma (EGG) distribution, which is valid for turbulence in the presence of air bubbles.

[1]Although NOMA systems are considered as future of wireless communication technologies, NOMA can also be combined with orthogonal multiple access (OMA) approaches. See for example hybrid orthogonal/non-orthogonal experimental indoor works [40], [41].

To the best of our knowledge, power domain NOMA for UVLC over lognormal turbulence channels was only addressed in [31], [34]. In [31], the effect of turbulence strength on the channel capacity in addition to the effect of targeted rate and number of nodes on coverage probability have been investigated. In [34], the effect of power allocation coefficient on the achievable capacity and coverage probability has been studied. Note that the above discussed contributions are limited to numerical evaluation, and lack the solid theoretical foundation and derivations.

Motivated by the earlier discussion, the main contributions of this paper are summarized as follows:

1) We derive a novel closed-form expression for the capacity of VLC NOMA system over a lognormal turbulence channel.
2) In an effort to gain more insight into the capacity performance of the underlying system model, we derive asymptotic closed-form capacity expressions, and demonstrate that the asymptotic capacity of the closest node to the clusterhead is the only node that is affected by underwater optical turbulence, i.e., the turbulence is encountered only in the asymptotic capacity of the first node. On the other hand, the asymptotic capacity of other nodes is controlled by the considered power allocation coefficient scheme.
3) To corroborate the efficiency of NOMA in underwater VLC systems, we present the achievable capacity of OFDMA scheme.
4) To further demonstrate the efficiency of NOMA system, we compare the achievable capacity in the presence and absence of underwater optical turbulence.
5) We present numerical and simulation results, with the aim to verify the derived mathematical framework and quantify the system performance under different scenarios, including different power allocation schemes, distances, and water types.

The remainder of the paper is organized as follows: In Section II, we present the considered system and channel models. In Section III, we present closed-form and asymptotic expressions for the system capacity over lognormal fading channels. In Section IV, we present the numerical results and finally conclude in Section V.

II. SYSTEM AND CHANNEL MODELS

We consider a NOMA-enabled UVLC where a clusterhead communicates with K underwater sensor nodes, as depicted in Fig. 1. Each node is assumed to be at a distance d_k, $k = 1, 2, \ldots, K$, from the clusterhead. Let P_T, x_k and α_k denote the available power budget shared by all nodes, the transmitted unipolar signal to the k^{th} node, and power allocation coefficient of the k^{th} node, respectively. Therefore, the allocated power to the k^{th} node is given by $P_k = \alpha_k P_T$. Power allocation coefficients are subject to the constraint of $\sum_{k=1}^{K} \alpha_k = 1$. It should be noted that splitting the transmit power with proper coefficients among nodes allows the practical realization of successive interference cancellation (SIC),

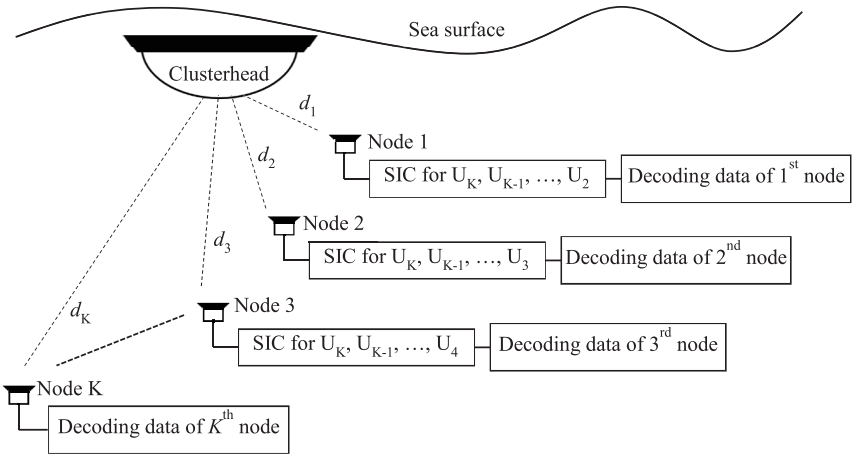

FIGURE 1. NOMA for downlink UVLC.

i.e., it increases the ability of the receiver to eliminate the effect of high power signals and perform reliable signal detection. In other words, the receiver can successively decode the higher power signals and consider all other signals as interference, subtract the decoded signal from the superimposed signal and finally detect the intended signal.

Mathematically, the transmitted signal from the clusterhead is given by $\mathcal{X} = \sum_{k=1}^{K} \sqrt{P_k}\, x_k$. The received signal at the k^{th} node is given by

$$y_k = \eta\, r\, h_k I_k\, \mathcal{X} + w_k, \tag{1}$$

where η is the laser diode's electro-optical conversion efficiency and r is the photodetector's opto-electrical responsivity. w_k is the additive white Gaussian noise (AWGN) term at the k^{th} receiver, $k = 1, 2, \ldots, K$. It has zero mean and a variance of $\sigma_n^2 = N_0 W$ where N_0 is the noise power spectral density and W is the system bandwidth. In (1), I_k, $k = 1, 2, \ldots, K$ are random variables characterizing the fading induced by the underwater turbulence, whereas h_k, $k = 1, 2, \ldots, K$ are deterministic terms that characterize the attenuation loss between the clusterhead and the k^{th} node, $k = 1, 2, \ldots, K$.

Under the assumption of semi-collimated laser sources with Gaussian beam shape, h_k is expressed as [11]

$$h_k \approx D_R^2 \theta_F^{-2} d_k^{-2} \exp\left(-c D_R^{\rho} \theta_F^{-\rho} d_k^{1-\rho}\right), \tag{2}$$

where θ_F and D_R denote full-width transmitter beam divergence angle and receiver aperture diameter, respectively. In (2), ρ and c represent correction and extinction coefficients, which are both dependent on water type [11]. Under the assumption of weak turbulence, the probability density function (PDF) of the fading coefficient is given by [6]

$$f_{I_k}(I_k) = \frac{1}{I_k \sqrt{2\pi\left(4\sigma_{x_k}^2\right)}} \exp\left(-\frac{\left(\ln(I_k) - 2\mu_{x_k}\right)^2}{2\left(4\sigma_{x_k}^2\right)}\right), \tag{3}$$

where μ_{x_k} and $\sigma_{x_k}^2$ denote the mean and variance of the log-amplitude coefficient, respectively. To ensure that the fading coefficient does not change the value of average power, the fading amplitude is normalized such that $\mathrm{E}[I_k] = 1$, which implies $\mu_{x_k} = -\sigma_{x_k}^2$ [44]. The variance can be written in terms of the scintillation index ($\sigma_{I_k}^2$) as $\sigma_{x_k}^2 = 0.25 \ln\left(\sigma_{I_k}^2 + 1\right)$. Scintillation index for laser sources with Gaussian beam shape can be calculated by [45, Eq. (7)] and [46, Eq. (16)].

Power allocation in NOMA systems is determined based on the channels condition between the transmitter and the receiving nodes. Specifically, nodes with strong channel gains (i.e., closest nodes to the clusterhead) are allocated lower power coefficients, while high power coefficients are assigned to nodes with weak channel gain. Without loss of generality, we assume that channel gains are ordered in a descending form, i.e., $h_1 > h_2 > \cdots > h_K$, hence the power allocation coefficients are then given as $\alpha_K > \cdots > \alpha_2 > \alpha_1$. Since the highest transmit power is assigned to the K^{th} node, this node does not perform SIC. On the other hand, since the least transmit power is assigned to the first node, this node will decode the data of $K-1$ nodes before decoding its own signal. The operation at the k^{th} SIC receiver can be described as follows. The receiver first detects/decodes the signal sent for the furthest point (i.e., K^{th} node). After detection/decoding it, k^{th} SIC receiver cancels the interference contributed by the K^{th} node. k^{th} SIC receiver repeats this processes, respectively, for $(K\text{-}1)^{\text{th}}$ node, $(K\text{-}2)^{\text{th}}$ node, …, $(k\text{+}1)^{\text{th}}$ node. k^{th} SIC receiver will finally decode/detect its own signal after canceling the effect of k+1, …, K nodes.

III. SUM CAPACITY ANALYSIS

The sum capacity of NOMA can be written as $R_T = \sum_{k=1}^{K} \overline{R_k}$. Due to the fact that the classical Shannon's equation does not work for optical systems, the exact capacity is still unknown for optical channel. Consequently, different bounds on capacity of optical channels were

derived [47]–[50]. Based on [50], the gap between the exact and lower bound on channel capacity can be efficiently neglected for high SNR and then the tight lower bound on capacity and assuming perfect SIC, the conditional capacity of the k^{th} node (conditioned on the fading coefficients I_k, $k = 1, 2, \ldots, K$) can be written as [2]

$$R_k \approx W \log_2 \left(1 + \frac{\exp(1)}{2\pi} \gamma_k \left(I_k^2\right)\right), \tag{4}$$

where $\gamma_k \left(I_k^2\right)$ is given as

$$\gamma_k \left(I_k^2\right) = \frac{P_k \eta^2 r^2 h_k^2 I_k^2}{N_0 W + \eta^2 r^2 h_k^2 I_k^2 \sum_{i=1}^{k-1} P_i}. \tag{5}$$

The average capacity can be calculated by averaging (4) over the PDF of the turbulence in (3) as (6), as shown at the bottom of the page. To solve the integral in (6), we apply a variable change $x = \ln(I_k)$. It can be noticed that x follows the normal distribution with mean $2\mu_{x_k}$ and variance $4\sigma_{x_k}^2$. Therefore, (6) can be expressed as

$$\overline{R_k} \approx E[g(x)] = \int_{-\infty}^{\infty} g(x) f_x(x) \, dx. \tag{7}$$

where $\mathrm{E}[\cdot]$ denotes the expectation operator. Here, $g(x)$ and $f_x(x)$ are defined, respectively, as

$$g(x) = W \log_2 \left(1 + \frac{\exp(1)}{2\pi} \gamma_k (\exp(2x))\right). \tag{8}$$

$$f_x(x) = \frac{1}{\sqrt{2\pi \left(4\sigma_{x_k}^2\right)}} \exp\left(-\frac{\left(x - 2\mu_{x_k}\right)^2}{2\left(4\sigma_{x_k}^2\right)}\right). \tag{9}$$

[2]**Note:** In the absence of underwater optical turbulence, the SNR for the k^{th} node is deterministic and found as $\gamma_k = P_k \eta^2 r^2 h_k^2 \Big/ \left(N_0 W + \eta^2 r^2 h_k^2 \sum_{i=1}^{k-1} P_i\right)$. Therefore, the capacity of the k^{th} node, in the absence of turbulence, can be calculated by (4) after replacing $\gamma_k \left(I_k^2\right)$ by γ_k.

Utilizing Holtzmann's Gaussian approximation [51], (7) can be approximated as weighted sum of $g(x)$ by replacing x with $2\mu_{x_k}$, $2\mu_{x_k} - 2\sqrt{3}\sigma_{x_k}$ and $2\mu_{x_k} + 2\sqrt{3}\sigma_{x_k}$ as (10), as shown at the bottom of the page.

In an effort to have further insight into the capacity, we pursue asymptotic analysis in the following. Applying the approximation $\mathrm{E}\left[\log_2\left(1 + a/b\right)\right] \approx \log_2\left(1 + \mathrm{E}[a]/\mathrm{E}[b]\right)$ [52, Eq. (35)], we can write (7) as

$$\overline{R_k} \approx W \log_2 \left(1 + \frac{\exp(1)}{2\pi} \gamma_k \left(\mathrm{E}\left[\exp(2x)\right]\right)\right), \tag{11}$$

It can be readily verified that $\mathrm{E}\left[\exp(2x)\right] = \exp\left(8\sigma_{x_k}^2 + 4\mu_{x_k}\right)$. Replacing this within (11), we have

$$\overline{R_k} \approx W \log_2 \left(1 + \frac{\exp(1)}{2\pi} \gamma_k \left(\exp\left(8\sigma_{x_k}^2 + 4\mu_{x_k}\right)\right)\right). \tag{12}$$

Noting that the inner argument of the exponential function in (12) is extremely small (i.e., $\left(8\sigma_{x_k}^2 + 4\mu_{x_k}\right) \ll 1$). Therefore, $\exp\left(8\sigma_{x_k}^2 + 4\mu_{x_k}\right)$ can be efficiently replaced by 1. This implies that the capacity of NOMA system in the presence of underwater optical turbulence is almost close to the capacity of NOMA system in the absence of underwater optical turbulence, i.e., $\overline{R_k} \approx W \log_2\left(1 + \left(\exp(1)/2\pi\right) \gamma_k(1)\right)$.

In the following, we consider asymptotically high transmit power, i.e., $P_T \to \infty$. It can be readily found that (12) reduces to (13), as shown at the bottom of the page.

The asymptotic capacity expression in (13) suggests that as P_T approaches ∞, the effect of turbulence is encountered only in the first node, which was demonstrated to have a low impact on the NOMA capacity. The asymptotic capacity of other nodes is determined by the power allocation coefficients. Therefore, it can be concluded that the system's asymptotic capacity in the presence of underwater optical turbulence is close to the asymptotic NOMA capacity in the absence of turbulence. In other words, despite the continuous changes in turbulence strength, the NOMA capacity remains

$$\overline{R_k} = \frac{W}{\sqrt{2\pi \left(4\sigma_{x_k}^2\right)}} \int_0^{\infty} \log_2 \left(1 + \frac{\exp(1)}{2\pi} \gamma_k \left(I_k^2\right)\right) I_k^{-1} \exp\left(-\frac{\left(\ln(I_k) - 2\mu_{x_k}\right)^2}{2\left(4\sigma_{x_k}^2\right)}\right) d_{I_k} \tag{6}$$

$$\begin{aligned}\overline{R_k} \approx{}& \frac{2}{3} W \log_2 \left(1 + \frac{\exp(1)}{2\pi} \gamma_k \left(\exp\left(4\mu_{x_k}\right)\right)\right) + \frac{1}{6} W \log_2 \left(1 + \frac{\exp(1)}{2\pi} \gamma_k \left(\exp\left(4\mu_{x_k} - 4\sqrt{3}\sigma_{x_k}\right)\right)\right) \\ &+ \frac{1}{6} W \log_2 \left(1 + \frac{\exp(1)}{2\pi} \gamma_k \left(\exp\left(4\mu_{x_k} + 4\sqrt{3}\sigma_{x_k}\right)\right)\right)\end{aligned} \tag{10}$$

$$\overline{R_k}_{P_T \to \infty} \approx \begin{cases} W \log_2 \left(\dfrac{\exp(1)}{2\pi} \dfrac{P_T \alpha_1 \eta^2 r^2 h_1^2 \exp\left(8\sigma_{x_1}^2 + 4\mu_{x_1}\right)}{N_0 W}\right), & k = 1 \\ W \log_2 \left(1 + \dfrac{\exp(1)}{2\pi} \dfrac{\alpha_k}{\sum_{i=1}^{k-1} \alpha_i}\right), & k = 2, 3, \ldots, K \end{cases} \tag{13}$$

almost constant. This further motivates the employment of NOMA as an efficient scheme for multi-access in underwater environments.

IV. NUMERICAL RESULTS

In this section, we present the capacity of wireless nodes in NOMA UVLC system. We also validate our derived closed-form expression in (10), closed-form approximate capacity expression in (12) and asymptotic capacity expression in (13). Unless mentioned otherwise, we consider a two sensor nodes scenario, $K = 2$, which is commonly adopted in the literature in order to ensure limited inter-user interference, e.g., [53]–[56]. We further consider receiver aperture diameter of $D_R = 5$ cm, full-width transmitter beam divergence angle of $\theta_F = 6°$, noise power spectral density of $N_0 = 10^{-22}$ W/Hz, a bandwidth of $W = 200$ MHz and total transmit power of $P_T = 1$ W. Assuming clear ocean and coastal water, the extinction and correction coefficients are given, respectively, as $(c, \rho) = (0.15, 0.05)$ and $(0.305, 0.13)$ [11]. Electro-optical efficiency of $\eta = 0.5$ W/A and opto-electrical responsivity of $r = 0.28$ A/W are considered. We further calculate the scintillation index (σ_I^2)[3] based on [45, Eq. (7)] in conjunction with [46, Eq. (16)] assuming salinity of 35 PPT and temperature of 20 °C.

In Fig. 2, we present the capacity of NOMA and discuss the effect of power allocation coefficient considering $d_T = d_1 + d_2 = 20$ m. Since d_1 is assumed to be shorter than d_2, we consider the range of $d_1 < d_T/2$. Since the received power at k^{th} node is proportional to h_k^2 and given the fact that power allocation coefficient is performed such that low transmits powers are assigned to the nodes with less severe channels and vice versa, we consider $\alpha_k \propto 1/h_k^2$, $k = 1, 2, \ldots, K$. Utilizing this and $\sum_{k=1}^{K} \alpha_k = 1$, we consider in simulation $\alpha_k = \left(1/h_k^2\right)/\sum_{i=1}^{K}\left(1/h_i^2\right)$, i.e., for two-node case $\alpha_1 = h_2^2/\left(h_1^2 + h_2^2\right)$ and $\alpha_2 = h_1^2/\left(h_1^2 + h_2^2\right)$. In order to demonstrate the efficiency of NOMA in underwater VLC networks, the sum capacity of NOMA in the absence of underwater optical turbulence is further included as a benchmark.

It can be observed from Fig. 2 that the derived expression in (10) provides excellent match to the analytical calculation based on (6). It can be noted that when $\alpha_1 = 0$, i.e., no power is allocated to the first node, its achievable capacity is zero. In this case, the second node achieves capacity of $R_2 = 9.57$ bps/Hz and $R_2 = 5.95$ bps/Hz for clear ocean and coastal water, respectively. This also indicates that the highest capacity for the second node in clear ocean is higher than its highest capacity in coastal water. This is due to the fact that the extinction coefficient of coastal water is higher than that of clear ocean, which results in weaker channel coefficient. It can be further observed that, when α_1 increases (i.e., $\alpha_2 = 1-\alpha_1$ decreases), the capacity of the first node increases and the capacity of the second node decreases. It is also noted that the capacity of the first node (i.e., R_1) approaches the NOMA overall capacity while the capacity of the second node (i.e., R_2) approaches zero as α_1 increases.

[3]For computing σ_I^2, we assume a dissipation rate of mean-squared temperature of 1×10^{-3} K^2s^{-3}, a dissipation rate of turbulent kinetic energy per unit mass of fluid of 1×10^{-2} m^2s^{-3}, relative strength of temperature, salinity fluctuation of $\omega = -3$ and wavelength of $\lambda = 530$ nm in [46].

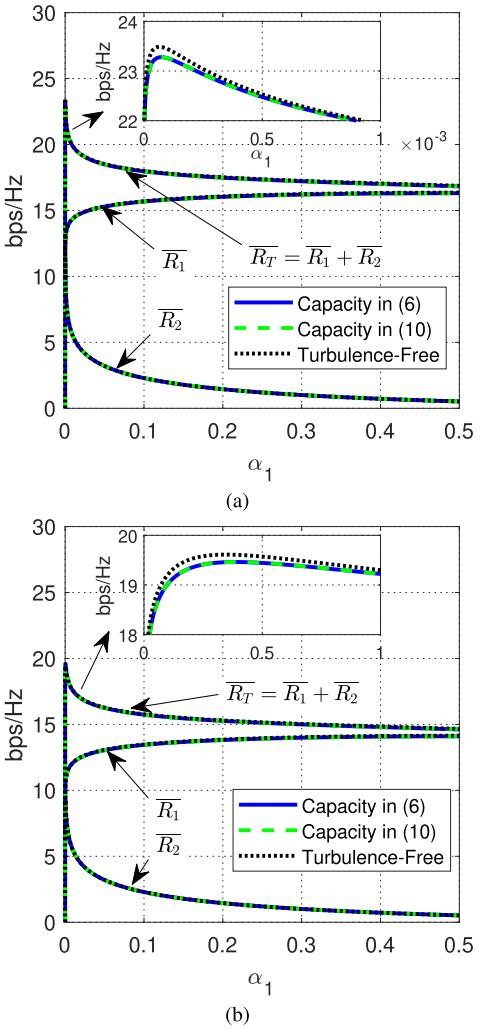

FIGURE 2. Capacity of downlink NOMA system with two nodes: (a) clear ocean and (b) coastal water.

On the other hand, the highest sum capacity is achieved for clear ocean when $\alpha_1 = 7.1901 \times 10^{-05}$ as $\overline{R_T} = 23.28$ bps/Hz. This corresponds to distances of $d_1 = 3.43$ m and $d_2 = 16.57$ m. For coastal water, the highest sum capacity is achieved when $\alpha_1 = 3.93 \times 10^{-04}$ as $\overline{R_T} = 19.46$ bps/Hz. This corresponds to distances of $d_1 = 5.084$ m and $d_2 = 14.916$ m. This indicates that the highest sum capacity in different water types requires different distances from the cluster head.

It can be further observed that the capacity of the NOMA system in the absence of underwater optical turbulence is slightly higher than the NOMA capacity in the presence of turbulence. This gives great importance to the deployment of NOMA system in an underwater environment. For example: While the highest sum capacity is achieved for clear ocean

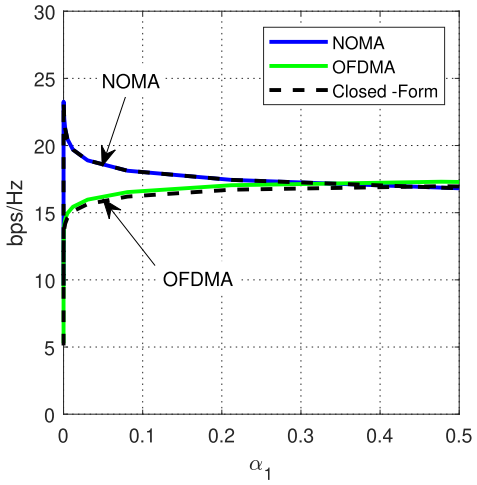

FIGURE 3. Capacity comparison between NOMA and OFDMA systems with two nodes.

as $\overline{R_T} = 23.28$ bps/Hz in the presence of under water optical turbulence, it is obtained as $\overline{R_T} = 23.49$ bps/Hz in the absence of turbulence. Moreover, the distribution of sensor nodes for achieving the best performance (i.e., highest capacity) of the NOMA system in the presence of under water optical turbulence and in the absence of it is almost the same if we consider the same water type. For example, if we consider clear ocean, the highest capacity that can be obtained in the presence of turbulence is achieved when the first node is placed at a distance of $d_1 = 3.43$ m and the second node at a distance of $d_2 = 16.57$ m meters. The distances for achieving the highest performance in the same water type and in the absence of turbulence are found as $d_1 = 3.37$ m and $d_2 = 16.63$ m. This in turn suggests that it is possible to use the NOMA system in an underwater environment by choosing fixed locations for user nodes, as long as the system is used in the same water type.

In order to demonstrate the superiority of NOMA underwater VLC communication, we consider two sensor nodes in a clear ocean and compare the capacity of NOMA system with OFDMA counterpart considering $d_T = d_1 + d_2 = 20$ m. It can be seen from Fig. 3 that, in most cases, the capacity of the NOMA system exceeds that of the OFDMA system. The capacity of the OFDMA system slightly exceeds the capacity of the NOMA system in cases where the user nodes are very close to each other. This is due to the high interference experienced in NOMA systems as users have almost the same channel coefficient and accordingly, close power coefficients are assigned to all nodes. It can be further observed that, while the highest capacity of NOMA system is obtained as $\overline{R_T} = 23.28$ bps/Hz when $d_1 = 3.43$ m and $d_2 = 16.57$ m, the highest capacity of OFDMA system is obtained as $\overline{R_T} = 17.31$ bps/Hz when $d_1 = d_2 = 10$ m.

In the following, we study the effect of distance difference on NOMA capacity considering coastal water. We assume that $d_T = d_1 + d_2$ is fixed and consider two cases: $d_T = 15$ m and $d_T = 20$ m in Figs. 4.a and 4.b, respectively. It can

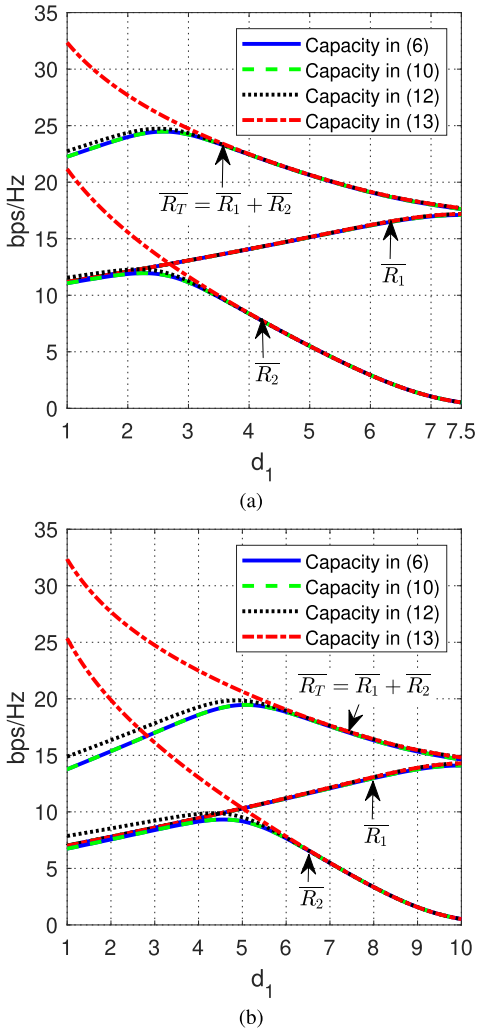

FIGURE 4. Effect of distance on the capacity of downlink NOMA with two nodes assuming coastal water: (a) $d_1 + d_2 = 15$ m and (b) $d_1 + d_2 = 20$ m.

be observed from Fig. 4 that, generally, the overall capacity increases as distance difference increases (i.e., $d_2 - d_1$ increases). This is because the power allocation coefficient for the farthest point is much larger than the power allocation coefficient for the nearest point (i.e., $\alpha_2 \gg \alpha_1$). Therefore, node 1 has a good capacity due to small propagation distance and node 2 has a good capacity due to very small interference from node 1. On the contrary, we observe a decrease in the overall capacity as d_1 increases, d_2 decreases and hence $d_2 - d_1$ decreases. This is due to the fact that the closer the nodes to each other the higher the interference.

The general observation of that the overall capacity increases as distance difference increases does not always hold as it can be observed from Figs. 4.a and 4.b that the maximum capacity is obtained when $d_1 = 2.59$ m and 5.07 m, respectively, for $d_1 + d_2 = 15$ m and 20 m. This is due to the fact that while assigning most of the power to the farthest point and very low amount of available power to the nearest point, the received power levels at both nodes are low. The nearest node to clusterhead receives a low power signal due

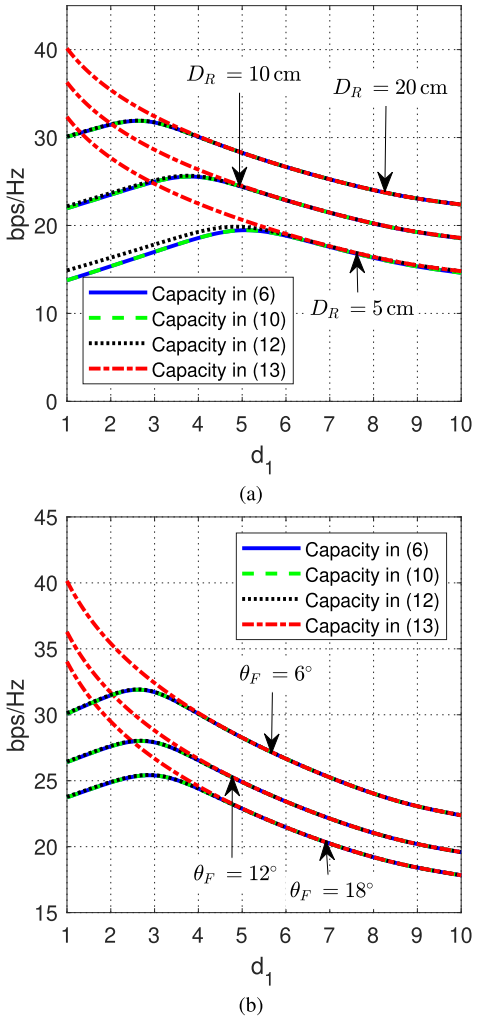

FIGURE 5. Effect of transceiver parameters on the capacity of downlink NOMA with two nodes assuming coastal water: (a) Effect of receiver aperture diameter and (b) Effect of transmitter beam divergence angle.

to assigning low power to it. At the same time, the furthest point receives a low signal power due to very weak channel coefficient.

It can also be observed in Fig. 4 that, although the transmit power is just 1 W, the asymptotic capacity expression in (12) which is derived assuming high transmit power (i.e., high SNR) provides good match with the exact capacity expression for some ranges of distances. These expressions deviate from the actual capacity for smaller d_1. because both nodes will have a low SNR. The first node will have low SNR since most of the power is assigned to the farthest node and the second node will have a low SNR due to very low channel gain that is strongly decaying with propagation distance. It can also be observed that the capacity of the first node increases with increasing d_1, This is due to the considered power allocation strategy. In other words, $P_1\eta^2\, r^2\, h_1^2$ increases with distance.

In the following, we investigate the effect of transceiver parameters on NOMA capacity considering coastal water and $d_T = 20$ m. Particularly, the effect of receiver aperture diameters and transmitter beam divergence angle on the achievable NOMA capacity have been investigated, respectively, in Figs. 5.a and 5.b.

For investigating the effect of receiver aperture diameters, $D_R = 5$ cm, 10 cm and 20 cm are assumed. The corresponding extinction coefficients are $\rho = 0.13$, 0.16 and 0.21, respectively [11, Table 1]. It is observed from Fig. 5.a that as receiver aperture size increases, the achievable NOMA capacity increases since larger receiver aperture sizes collect more energy. Furthermore, the larger aperture size, the less turbulence strength, yielding higher SNR. For example, at distance of $d_1 = 5$ m, aperture diameter of 10 cm and 20 cm provides, respectively, 25.33% and 45.22% improvement over aperture diameters of 5 cm. The important point is how aperture diameters affect on the optimal distance where maximum sum capacity is achieved. It can be observed from Fig. 5.a that the maximum sum capacity is obtained for $D_R = 5$ cm, 10 cm and 20 cm, respectively, at distance of $d_1 = 5.07$ m, 3.80 m, and $= 2.63$ m. Indicating that, the smaller the aperture diameter, the closer the nodes to each other which are found as $d_2 - d_1 = 9.86$ m, 12.4 m and 14.74 m, respectively. This is due to the need to reduce the distance of the second node from the clusterhead (i.e., d_2) when the receiving area is small in order to be able to receive a suitable power, given that the power received on the small area in the large distance is very little, and therefore the second point will have a very small SNR.

For investigating the effect of transmitter's beam divergence angle, $\theta_F = 6°$, 12° and 18° are assumed. The corresponding extinction coefficients are $\rho = 0.21$, 0.24 and 0.25, respectively [11, Table 1]. It can be observed from Fig. 5.b that as divergence angle increases, the achievable NOMA capacity decreases. This is due to the fact that the focused beam (i.e., more collimated angle) experiences less attenuation and less geometric loss through the propagation medium. For example, the achievable NOMA capacity in coastal water at distance of $d_1 = 5$ m and beam divergence angle of $\theta_F = 6°$ provides 8.83% and 23.57% higher capacity over beam divergence angle of $\theta_F = 12°$ and $\theta_F = 18°$, respectively. The important point is how transmitter's beam divergence angles affect on the optimal distance where maximum sum capacity is achieved. It can be observed from Fig. 5. b that the maximum sum capacity is obtained for $\theta_F = 6°$, 12° and 18°, respectively, at distance of $d_1 = 2.63$ m, 2.69 m, and $= 2.87$ m. Indicating that, the larger the transmitter's beam divergence angles, the closer the nodes to each other which are found as $d_2 - d_1 = 14.74$ m, 14.62 m and 14.26 m, respectively. Unlike the effect of aperture diameter on the optimal locations of nodes, the effect of transmitter's beam divergence angles is quite negligible.

In all of the above results, we considered the scenario of two sensor nodes. In the following, we study the presence of a number of sensor nodes on the NOMA sum capacity assuming coastal water and $d_T = \sum_{k=1}^{K} d_k = 20$ m. Particularly, we have tabulated the maximum sum capacity that can be achieved in each case, as well as the distances of sensor nodes from the clusterhead and power allocation coefficients

TABLE 1. Maximum sum capacity of NOMA downlink with K nodes ($d_T = 20$ m and Coastal water are assumed).

Sensor Nodes (K)	2	3	4	5
Power allocation coefficients: $(\alpha_k, k = 1, 2, \cdots, K)$ **& Distances from the clusterhead:** $(d_k, k = 1, 2, \cdots, K)$	$\alpha_1 = 3.93 \times 10^{-04}$ $d_1 = 5.084$ m	$\alpha_1 = 2.60 \times 10^{-08}$ $d_1 = 0.6372$ m	$\alpha_1 = 3.0737 \times 10^{-13}$ $d_1 = 0.0226$ m	$\alpha_1 = 1.8880 \times 10^{-17}$ $d_1 = 0.0027$ m
	$\alpha_2 = 0.9996$ $d_2 = 14.916$ m	$\alpha_2 = 1.0 \times 10^{-03}$ $d_2 = 5.4041$ m	$\alpha_2 = 1.6573 \times 10^{-06}$ $d_2 = 0.9575$ m	$\alpha_2 = 4.8521 \times 10^{-11}$ $d_2 = 0.1060$ m
		$\alpha_3 = 0.9990$ $d_3 = 13.9587$ m	$\alpha_3 = 0.3636$ $d_3 = 9.1513$ m	$\alpha_3 = 1.2260 \times 10^{-06}$ $d_3 = 1.1634$ m
			$\alpha_4 = 0.6364$ $d_4 = 9.8686$ m	$\alpha_4 = 0.0119$ $d_4 = 6.6046$ m
				$\alpha_5 = 0.9881$ $d_5 = 12.1234$ m
$\overline{R_T}$ bps/Hz	**19.46**	**30.69**	**44.33**	**55.02**

TABLE 2. Comparing the highest sum capacity of NOMA system with two hypothetical cases ($d_T = 20$ m and Coastal water are assumed).

Sensor Nodes (K)	$\overline{R_T}$ bps/Hz		
	Optimal	Case I	Case II
2	19.46	18.00	14.62
3	30.69	22.85	18.45
4	44.33	25.72	20.82
5	55.02	27.76	22.51

in Table 1. It can be seen that the sum capacity increases as the number of sensor nodes increases. It may be intuitive that increasing the number of sensor nodes increases the capacity. But the capacity does not increase if a new sensor node is added randomly. Rather, all sensor nodes must be redistributed with new distances from the clusterhead and with new power allocation coefficients. Otherwise, adding a new sensor node without re-allocating the old sensor nodes may increase the interference and hence decrease the sum capacity. In other words, adding additional sensor node requires changing the location of other sensor nodes and accordingly the power allocation coefficients. For example, while the maximum sum capacity for the case of two sensor nodes (i.e., $K = 2$) is obtained for $d_1 = 5.048$ m and $d_2 = 14.916$ m, the maximum sum capacity for four sensor nodes is achieved when $d_1 = 0.0226$ m, $d_2 = 0.9575$ m, $d_3 = 9.1513$ m and $d_4 = 9.8686$ m.

In the following, we assume coastal water and $d_T = \sum_{k=1}^{K} d_k = 20$ m and compare the highest sum capacity of NOMA system with two hypothetical cases, namely when the sensor nodes are separated from each other by the same distance (i.e., $d_{k+1} - d_k = \text{Constant}$, $k = 1, \ldots, K$) and when all sensor nodes are equidistant from the clusterhead (i.e., $d_i = d_k$, $k = 1, \ldots, K$ and, $i = 1, \ldots, K$).

It is noted that, regardless of the number of sensor nodes, the achieved sum capacity in the optimal placement of sensor nodes, given in Table 1, is the highest, while the lowest sum capacity is experienced when all nodes are equidistant from the clusterhead. This is due to the fact that, when sensor nodes are separated from each other by the same distance, the distances of the sensor nodes from the clusterhead are not the same; therefore it can achieve higher sum capacity than second hypothetical case, in which sensor nodes have the same distance from the clusterhead. For example, assume the presence of 5 sensor nodes, the sum capacity of the optimal case is evaluated to 55.02 bps/Hz. This value drops to 27.76 bps/Hz and 22.51 bps/Hz, respectively, for case I in which the sensor nodes are separated from each other by the same distance and case II in which all sensor nodes are equidistant from the clusterhead.

V. CONCLUSION

In this paper, we considered NOMA in the context of underwater sensor networks. To this end, we derived a simple closed-form expression for the NOMA capacity as well as a simple and accurate asymptotic representation. The derived closed-form expressions are in agreement with the corresponding analytic results, while they are insightful and easy to compute.

Analyzing the performance of the considered underwater network set up, we considered various scenarios where we studied the effect of different link distances on the overall NOMA capacity. We observed that the overall capacity is severely worsening with propagation distance which is due to the fact that the VLC channel gain severely drops with propagation distance. Therefore, the considered configuration can exhibit particularly high rates in the context of a local area network. We also compared the performance of the NOMA system with and without the presence of underwater optical disturbance. The results, as well as the theoretical study, proved that the NOMA system exhibits robust capacity performance in the presence and absence of an optical turbulence. This is because the capacity of most nodes depends mainly on the power allocation coefficient.

We further investigated the effect of system parameters on the optimal N nodes' distances, where maximum sum capacity is achieved. It is observed that while aperture diameters hugely influence the optimal distances where maximum sum

$$\overline{R_{k_{\text{OFDMA}}}} \approx \frac{2}{3} W_k \log_2\left(1+\frac{\exp(1)}{2\pi}\gamma_{k_{\text{OFDMA}}}\left(\exp\left(4\mu_{x_k}\right)\right)\right) + \frac{1}{6} W_k \log_2\left(1+\frac{\exp(1)}{2\pi}\gamma_{k_{\text{OFDMA}}}\left(\exp\left(4\mu_{x_k}-4\sqrt{3}\sigma_{x_k}\right)\right)\right) + \frac{1}{6} W_k \log_2\left(1+\frac{\exp(1)}{2\pi}\gamma_{k_{\text{OFDMA}}}\left(\exp\left(4\mu_{x_k}+4\sqrt{3}\sigma_{x_k}\right)\right)\right) \quad \text{(A3)}$$

capacity is achieved, the transmitter's beam divergence angle has almost negligible effect on the optimal nodes' distances. Additionally, one of the valuable observations that must be taken into account is that, for asymptotic analysis, the turbulence is encountered only in the first node and does not affect other nodes. The asymptotic capacity of other nodes is controlled by the power allocation coefficients.

APPENDIX

In order to demonstrate the superiority of NOMA system for achieving the highest capacity as a multiple access technique in an underwater environment, as benchmark, we need to compare it with the well-known multiple access technique of OFDMA. Since in OFDMA rather than sharing the whole bandwidth with all users/sensor nodes similar to the NOMA system, part of the bandwidth is assigned to each user (i.e., users are assigned to a group of subcarriers), we assume that bandwidth is shared among all users equally. For fair comparison with NOMA system counterpart, the same power allocation coefficient is assumed and hence the conditional capacity of the k^{th}, $k = 1, 2, \ldots, K$ node in OFDMA system can be written as

$$R_{k_{\text{OFDMA}}} \approx W_k \log_2\left(1+\frac{\exp(1)}{2\pi}\gamma_{k_{\text{OFDMA}}}\left(I_k^2\right)\right), \quad \text{(A1)}$$

where W_k is the assigned bandwidth for the k^{th} user and given as $W_k = W/k$. In (A1), $\gamma_{k_{\text{OFDMA}}}\left(I_k^2\right)$ is given as

$$\gamma_{k_{\text{OFDMA}}}\left(I_k^2\right) = \frac{P_k \eta^2 r^2 h_k^2 I_k^2}{N_0 W_k}. \quad \text{(A2)}$$

Similar to the average capacity of NOMA system over log-normal turbulence channel, Holtzmann's Gaussian approximation in [51] is used. The average capacity per user is then found as (A3), as shown at the top of the page.

REFERENCES

[1] C. M. G. Gussen, P. S. R. Diniz, M. L. R. Campos, W. A. Martins, and J. N. Gois, "A survey of underwater wireless communication technologies," *J. Commun. Inf. Sys.*, vol. 31, no. 1, pp. 242–255, 2016.

[2] Z. Zeng, S. Fu, H. Zhang, Y. Dong, and J. Cheng, "A survey of underwater optical wireless communications," *IEEE Commun. Surveys Tuts.*, vol. 19, no. 1, pp. 204–238, 1st Quart., 2017.

[3] D. C. Sigee, *Freshwater Microbiology: Biodiversity and Dynamic Interactions of Microorganisms in the Aquatic Environment*. Hoboken, NJ, USA: Wiley, Jun. 2005.

[4] A. P. Klimley, *The Biology of Sharks and Rays*. Chicago, IL, USA: Univ. of Chicago Press, 2013.

[5] C. Wang, H.-Y. Yu, Y.-J. Zhu, and T. Wang, "Blind detection for SPAD-based underwater VLC system under P–G mixed noise model," *IEEE Commun. Lett.*, vol. 21, no. 12, pp. 2602–2605, Dec. 2017.

[6] A. Tabeshnezhad and M. A. Pourmina, "Outage analysis of relay-assisted underwater wireless optical communication systems," *Opt. Commun.*, vol. 405, pp. 297–305, Sep. 2017.

[7] T. Shafique, O. Amin, M. Abdallah, I. S. Ansari, M.-S. Alouini, and K. Qaraqe, "Performance analysis of single-photon avalanche diode underwater VLC system using ARQ," *IEEE Photon. J.*, vol. 9, no. 5, pp. 1–11, Oct. 2017.

[8] S. Hessien, S. C. Tokgoz, N. Anous, A. Boyaci, M. Abdallah, and K. A. Qaraqe, "Experimental evaluation of OFDM-based underwater visible light communication system," *IEEE Photon. J.*, vol. 10, no. 5, pp. 1–13, Oct. 2018.

[9] G. Cossu, A. Sturniolo, A. Messa, D. Scaradozzi, and E. Ciaramella, "Full-fledged 10Base-T Ethernet underwater optical wireless communication system," *IEEE J. Sel. Areas Commun.*, vol. 36, no. 1, pp. 194–202, Jan. 2018.

[10] Z. Vali, A. Gholami, Z. Ghassemlooy, M. Omoomi, and D. Michelson, "Experimental study of the turbulence effect on underwater optical wireless communications," *Appl. Opt.*, vol. 57, no. 28, pp. 8314–8319, Oct. 2018.

[11] M. Elamassie, F. Miramirkhani, and M. Uysal, "Performance characterization of underwater visible light communication," *IEEE Trans. Commun.*, vol. 67, no. 1, pp. 543–552, Jan. 2019.

[12] N. Huang, M. Chen, W. Xu, and J.-Y. Wang, "Incorporating importance sampling in EM learning for sequence detection in SPAD underwater OWC," *IEEE Access*, vol. 7, pp. 4529–4537, 2019.

[13] N. Saeed, A. Celik, T. Y. Al-Naffouri, and M.-S. Alouini, "Localization of energy harvesting empowered underwater optical wireless sensor networks," *IEEE Trans. Wireless Commun.*, vol. 18, no. 5, pp. 2652–2663, May 2019.

[14] A. Yilmaz, M. Elamassie, and M. Uysal, "Diversity gain analysis of underwater vertical MIMO VLC links in the presence of turbulence," in *Proc. IEEE Int. Black Sea Conf. Commun. Netw. (BlackSeaCom)*, Jun. 2019, pp. 1–6.

[15] Y. Lou, J. Cheng, D. Nie, and G. Qiao, "Performance of underwater wireless optical communications in presents of cascaded mixture exponential-generalized gamma turbulence," 2020, *arXiv:2008.02868*. [Online]. Available: https://arxiv.org/abs/2008.02868

[16] E. Zedini, A. Kammoun, H. Soury, M. Hamdi, and M.-S. Alouini, "Performance analysis of dual-hop underwater wireless optical communication systems over mixture exponential-generalized gamma turbulence channels," *IEEE Trans. Commun.*, vol. 68, no. 9, pp. 5718–5731, Sep. 2020.

[17] M. Elamassie and M. Uysal, "Vertical underwater visible light communication links: Channel modeling and performance analysis," *IEEE Trans. Wireless Commun.*, vol. 19, no. 10, pp. 6948–6959, Oct. 2020.

[18] H. Jiang, H. Qiu, N. He, W. Popoola, Z. Ahmad, and S. Rajbhandari, "Performance of spatial diversity DCO-OFDM in a weak turbulence underwater visible light communication channel," *J. Lightw. Technol.*, vol. 38, no. 8, pp. 2271–2277, Apr. 15, 2020.

[19] Y.-W. Ji, G.-F. Wu, and C. Wang, "Generalized likelihood block detection for SPAD-based underwater VLC system," *IEEE Photon. J.*, vol. 12, no. 1, pp. 1–10, Feb. 2020.

[20] M. Chen, P. Zou, L. Zhang, and N. Chi, "Demonstration of a 2.34 Gbit/s real-time single silicon-substrate blue LED-based underwater VLC system," *IEEE Photon. J.*, vol. 12, no. 1, pp. 1–11, Feb. 2020.

[21] A. Uppalapati, R. P. Naik, and P. Krishnan, "Analysis of M-QAM modulated underwater wireless optical communication system for reconfigurable UOWSNs employed in river meets ocean scenario," *IEEE Trans. Veh. Technol.*, vol. 69, no. 12, pp. 15244–15252, Dec. 2020.

[22] Y. Kim, S. Arya, and Y. H. Chung, "An optimal energy harvesting scheme for simultaneous lightwave information and power transfer over multi-layer turbulence-induced underwater channel," *Opt. Commun.*, vol. 501, Dec. 2021, Art. no. 127382.
[23] A. A. E.-R. El-Fikky, E. M. Eldin, A. H. Fayed, A. A. E. Aziz, M. H. H. Shalaby, and H. M. Aly, "NLoS underwater VLC system performance: Static and dynamic channel modeling," *Appl. Opt.*, vol. 58, no. 30, pp. 8272–8281, Oct. 2019.
[24] A. M. Ghonim, W. M. Salama, A. E.-R. A. El-Fikky, A. A. M. Khalaf, and H. M. H. Shalaby, "Underwater localization system based on visible-light communications using neural networks," *Appl. Opt.*, vol. 60, no. 13, pp. 3977–3988, May 2021.
[25] Y. Kim, S. Arya, and Y. H. Chung, "An optimal energy harvesting scheme for simultaneous lightwave information and power transfer over multi-layer turbulence-induced underwater channel," *Opt. Commun.*, vol. 501, Dec. 2021, Art. no. 127382. [Online]. Available: https://www.sciencedirect.com/science/article/pii/S0030401821006313
[26] F. Miramirkhani, M. Karbalayghareh, and M. Uysal, "Effect of scattering phase function on underwater visible light communication channel models," *Phys. Commun.*, vol. 48, Oct. 2021, Art. no. 101410.
[27] Y. Inoue, T. Kodama, and T. Kimura, "Global optimization of relay placement for seafloor optical wireless networks," *IEEE Trans. Wireless Commun.*, vol. 20, no. 3, pp. 1801–1815, Mar. 2021.
[28] A. S. Ghazy, S. Hranilovic, and M.-A. Khalighi, "Angular MIMO for underwater wireless optical communications: Link modeling and tracking," *IEEE J. Ocean. Eng.*, vol. 46, no. 4, pp. 1391–1407, Oct. 2021.
[29] I. C. Ijeh, M. A. Khalighi, and S. Hranilovic, "Parameter optimization for an underwater optical wireless vertical link subject to link misalignments," *IEEE J. Ocean. Eng.*, vol. 46, no. 4, pp. 1424–1437, Oct. 2021.
[30] A. Amantayeva, M. Yerzhanova, and R. C. Kizilirmak, "Multiuser MIMO for underwater visible light communication," in *Proc. Int. Conf. Comput. Netw. Commun. (CoCoNet)*, Aug. 2018, pp. 164–168.
[31] C. Geldard, J. Thompson, and W. O. Popoola, "A study of non-orthogonal multiple access in underwater visible light communication systems," in *Proc. IEEE 87th Veh. Technol. Conf. (VTC Spring)*, Jun. 2018, pp. 1–6.
[32] M. Li and Y. Xiang, "A photon counting underwater NOMA wireless optical communication system," in *Proc. 7th Int. Conf. Inf., Commun. Netw. (ICICN)*, Apr. 2019, pp. 120–124.
[33] M. Elamassie, M. Karbalayghareh, F. Miramirkhani, M. Uysal, M. Abdallah, and K. Qaraqe, "Resource allocation for downlink OFDMA in underwater visible light communications," in *Proc. IEEE Int. Black Sea Conf. Commun. Netw. (BlackSeaCom)*, Jun. 2019, pp. 1–6.
[34] L. Zhang, Y. Chen, K. Zhang, J. Quan, Z. Li, and Y. Dong, "On performance of multiuser underwater wireless optical communication systems," in *Proc. Int. Conf. Comput., Netw. Commun. (ICNC)*, Feb. 2020, pp. 1042–1046.
[35] M. Jain, N. Sharma, A. Gupta, D. Rawal, and P. Garg, "Performance analysis of NOMA assisted underwater visible light communication system," *IEEE Wireless Commun. Lett.*, vol. 9, no. 8, pp. 1291–1294, Aug. 2020.
[36] L. Zhang, Z. Wang, Z. Wei, Y. Dong, H. Y. Fu, and J. Cheng, "High-speed multi-user underwater wireless optical communication system based on NOMA scheme," in *Proc. 14th Pacific Rim Conf. Lasers Electro-Opt. (CLEO PR)*, 2020, pp. 1–2.
[37] D. Chen, Y. Wang, J. Jin, H. Lu, and J. Wang, "An experimental study of NOMA in underwater visible light communication system," *Opt. Commun.*, vol. 475, Nov. 2020, Art. no. 126199.
[38] M. Jain, N. Sharma, A. Gupta, D. Rawal, and P. Garg, "NOMA assisted underwater visible light communication system with full-duplex cooperative relaying," *Veh. Commun.*, vol. 31, Oct. 2021, Art. no. 100359.
[39] R. Jiang, C. Sun, X. Tang, L. Zhang, H. Wang, and A. Zhang, "Joint user-subcarrier pairing and power allocation for uplink ACO-OFDM-NOMA underwater visible light communication systems," *J. Lightw. Technol.*, vol. 39, no. 7, pp. 1997–2007, Apr. 1, 2021.
[40] B. Lin, W. Ye, X. Tang, and Z. Ghassemlooy, "Experimental demonstration of bidirectional NOMA-OFDMA visible light communications," *Opt. Exp.*, vol. 25, no. 4, pp. 4348–4355, Feb. 2017.
[41] A. Adnan, Y. Liu, C.-W. Chow, and C.-H. Yeh, "Demonstration of non-hermitian symmetry (NHS) IFFT/FFT size efficient OFDM non-orthogonal multiple access (NOMA) for visible light communication," *IEEE Photon. J.*, vol. 12, no. 3, pp. 1–5, Jun. 2020.
[42] Z. Ding, X. Lei, G. K. Karagiannidis, R. Schober, J. Yuan, and V. Bhargava, "A survey on non-orthogonal multiple access for 5G networks: Research challenges and future trends," *IEEE J. Sel. Areas Commun.*, vol. 35, no. 10, pp. 2181–2195, Oct. 2017.
[43] M. V. Jamali, A. Mirani, A. Parsay, B. Abolhassani, P. Nabavi, A. Chizari, P. Khorramshahi, S. Abdollahramezani, and J. A. Salehi, "Statistical studies of fading in underwater wireless optical channels in the presence of air bubble, temperature, and salinity random variations," *IEEE Trans. Commun.*, vol. 66, no. 10, pp. 4706–4723, May 2018.
[44] S. M. Navidpour, M. Uysal, and M. Kavehrad, "BER performance of free-space optical transmission with spatial diversity," *IEEE Trans. Wireless Commun.*, vol. 6, no. 8, pp. 2813–2819, Aug. 2007.
[45] M. Cheng, L. Guo, and Y. Zhang, "Scintillation and aperture averaging for Gaussian beams through non-Kolmogorov maritime atmospheric turbulence channels," *Opt. Exp.*, vol. 23, no. 25, pp. 32606–32621, Dec. 2015.
[46] M. Elamassie, M. Uysal, Y. Baykal, M. Abdallah, and K. Qaraqe, "Effect of eddy diffusivity ratio on underwater optical scintillation index," *J. Opt. Soc. Amer. A, Opt. Image Sci.*, vol. 34, no. 11, pp. 1969–1973, 2017.
[47] A. Lapidoth, S. M. Moser, and M. A. Wigger, "On the capacity of free-space optical intensity channels," *IEEE Trans. Inf. Theory*, vol. 55, no. 10, pp. 4449–4461, Oct. 2009.
[48] J.-B. Wang, Q.-S. Hu, J. Wang, M. Chen, and J.-Y. Wang, "Tight bounds on channel capacity for dimmable visible light communications," *J. Lightw. Technol.*, vol. 31, no. 23, pp. 3771–3779, Dec. 1, 2013.
[49] A. Chaaban, J.-M. Morvan, and M.-S. Alouini, "Free-space optical communications: Capacity bounds, approximations, and a new sphere-packing perspective," *IEEE Trans. Commun.*, vol. 64, no. 3, pp. 1176–1191, Mar. 2016.
[50] L. Yin and H. Haas, "Physical-layer security in multiuser visible light communication networks," *IEEE J. Sel. Areas Commun.*, vol. 36, no.1, pp. 162–174, Jan. 2018.
[51] J. M. Holtzmann, "On using perturbation analysis to do sensitivity analysis: Derivatives versus differences," *IEEE Trans. Autom. Control*, vol. 37, no. 2, pp. 243–247, Feb. 1992.
[52] E. Bjornson, M. Matthaiou, and M. Debbah, "A new look at dual-hop relaying: Performance limits with hardware impairments," *IEEE Trans. Commun.*, vol. 61, no. 11, pp. 4512–4525, Nov. 2013.
[53] R. C. Kizilirmak, C. R. Rowell, and M. Uysal, "Non-orthogonal multiple access (NOMA) for indoor visible light communications," in *Proc. 4th Int. Workshop Opt. Wireless Commun. (IWOW)*, Sep. 2015, pp. 98–101.
[54] Z. Ding, R. Schober, and H. V. Poor, "On the impact of phase shifting designs on IRS-NOMA," *IEEE Wireless Commun. Lett.*, vol. 9, no. 10, pp. 1596–1600, Oct. 2020.
[55] Z. Ding, H. Dai, and H. V. Poor, "Relay selection for cooperative NOMA," *IEEE Wireless Commun. Lett.*, vol. 5, no. 4, pp. 416–419, Aug. 2016.
[56] F. Fang, Y. Xu, Q.-V. Pham, and Z. Ding, "Energy-efficient design of IRS-NOMA networks," *IEEE Trans. Veh. Technol.*, vol. 69, no. 11, pp. 14088–14092, Nov. 2020.

MOHAMMED ELAMASSIE (Senior Member, IEEE) received the B.Sc. and M.Sc. degrees in electrical engineering from the Islamic University of Gaza, Gaza Strip, Palestine, in 2006 and 2011, respectively, and the Ph.D. degree in electrical and electronics engineering from Özyeğin University, Istanbul, Turkey, in June 2020.

He has several practical experiences serving as a Designing and Supervising Electrical Engineer with the Engineering Office and Development Department, Ministry of Health, Gaza, Palestine, for four years. His current research interests include visible light communications, optical turbulence, underwater acoustic communication, diversity techniques for fading channels, performance analysis over fading channels and time-varying channels, channel estimation and equalization, multi-input multi-output (MIMO) communications. On these topics, he has authored more than 28 publications (journals and conferences) and received more than 300 Google Scholar citations with an H-index of 10.

Dr. Elamassie's major achievements include the Best Paper Award in IEEE International Black Sea Conference on Communications and Networking, Sochi, Russia, in 2019. He also received the 2020 IEEE Turkey Doctoral Thesis Award. He is a Review Editor on the Editorial Board of Non-Conventional Communications and Networks (specialty section of Frontiers in Communications and Networks). He is also a Review Editor on the Editorial Board of Wireless Communications (specialty section of Frontiers in Communications and Networks). He has served as a Reviewer for the Institute of Electrical and Electronics Engineers (IEEE) and the Optical Society of America (OSA) journals and conferences as well.

LINA BARIAH (Senior Member, IEEE) received the M.Sc. and Ph.D. degrees in communications engineering from Khalifa University, Abu Dhabi, United Arab Emirates, in 2015 and 2018, respectively. She was a Visiting Researcher with the Department of Systems and Computer Engineering, Carleton University, Ottawa, ON, Canada, in 2019. She is currently a Postdoctoral Fellow with the KU Center for Cyber-Physical Systems, Khalifa University, and an Affiliate Research Fellow with the James Watt School of Engineering, University of Glasgow, U.K. Her research interests include advanced digital signal processing techniques for communications, machine learning, cooperative communications, non-orthogonal multiple access, cognitive radios, reconfigurable intelligent surfaces, aerial networks, and visible light communications. She was a Technical Program Committee Member of a number of IEEE conferences, such as ICC and Globecom. She is an Associate Editor for the IEEE Open Journal of the Communications Society and an Area Editor for *Physical Communication* (Elsevier). She is a Guest Editor of *RS Open Journal on Innovative Communication Technologies* (RS-OJICT). She serves as the session chair and an active reviewer for numerous IEEE conferences and journals.

MURAT UYSAL (Fellow, IEEE) received the B.Sc. and M.Sc. degrees in electronics and communication engineering from Istanbul Technical University, Istanbul, Turkey, in 1995 and 1998, respectively, and the Ph.D. degree in electrical engineering from Texas A&M University, College Station, TX, USA, in 2001.

He is currently a Full Professor and the Chair of the Department of Electrical and Electronics Engineering, Özyeğin University, Istanbul. He also serves as the Founding Director for the Center of Excellence in Optical Wireless Communication Technologies (OKATEM). Prior to joining Özyeğin University, he was a Tenured Associate Professor with the University of Waterloo, Canada. His research interests include the broad area of communication theory, with a particular emphasis on the physical layer aspects of wireless communication systems in radio and optical frequency bands. On these topics, he has authored some 350 journal articles and conference papers and received more than 14.000 citations with an H-index of 56.

Prof. Uysal's major distinctions include the NSERC Discovery Accelerator Award, in 2008, the University of Waterloo Engineering Research Excellence Award, in 2010, the Turkish Academy of Sciences Distinguished Young Scientist Award, in 2011, the Özyeğin University Best Researcher Award, in 2014, the National Instruments Engineering Impact Award, in 2017, the Elginkan Foundation Technology Award, in 2018, and the IEEE Communications Society Best Survey Paper Award, in 2019, among others. He is the Former Chair of the IEEE Turkey Section. In particular, he served as the Technical Program Committee Chair for major IEEE conferences, including WCNC 2014, PIMRC 2019, and VTC-Fall 2019. He serves on the Editorial Board for IEEE Transactions on Wireless Communications. In the past, he has served as an Editor for IEEE Transactions on Communications, IEEE Transactions on Vehicular Technology, and IEEE Communications Letters. He was involved in the organization of several IEEE conferences at various levels.

SAMI MUHAIDAT (Senior Member, IEEE) received the Ph.D. degree in electrical and computer engineering from the University of Waterloo, Waterloo, in 2006. From 2007 to 2008, he was an NSERC Postdoctoral Fellow with the Department of Electrical and Computer Engineering, University of Toronto, Canada. From 2008 to 2012, he was an Assistant Professor with the School of Engineering Science, Simon Fraser University, BC, Canada. He is currently a Professor with Khalifa University and an Adjunct Professor with Carleton University, Canada. His research interests include advanced digital signal processing techniques for wireless communications, RIS, 5G and beyond, MIMO, optical communications, the IoT with emphasis on battery-free devices, and machine learning. He served as a Senior Editor and an Editor for the IEEE Communications Letters, an Editor of the IEEE Transactions on Communications, and an Associate Editor for the IEEE Transactions on Vehicular Technology. He is an Area Editor of the IEEE Transactions on Communications and a Lead Guest Editor of the IEEE Open Journal of the Communications Society (OJ-COMS) "Large-Scale Wireless Powered Networks with Backscatter Communications" Special Issue.

PASCHALIS C. SOFOTASIOS (Senior Member, IEEE) was born in Volos, Greece, in 1978. He received the M.Eng. degree from Newcastle University, U.K., in 2004, the M.Sc. degree from the University of Surrey, U.K., in 2006, and the Ph.D. degree from the University of Leeds, U.K., in 2011. He has held academic positions at the University of Leeds, the University of California at Los Angeles, CA, USA, the Tampere University of Technology, Finland, the Aristotle University of Thessaloniki, Greece, and the Khalifa University of Science and Technology, United Arab Emirates, where he currently serves as an Associate Professor for the Department of Electrical Engineering and Computer Science. His M.Sc. studies were funded by a scholarship from UKEPSRC and his Ph.D. studies were sponsored by UK-EPSRC and Pace plc. His research interests include the broad areas of digital and optical wireless communications as well as in topics relating to mathematical analysis and statistics. He received the Exemplary Reviewer Award from the IEEE Communications Letters, in 2012, and the IEEE Transactions on Communications, in 2015 and 2016. He received the Best Paper Award at ICUFN 2013. He serves as an Editor for the IEEE Communications Letters. He serves as a regular reviewer for several international journals and has been a member of the technical program committee of numerous IEEE conferences.